6698–6714 *Nucleic Acids Research, 2013, Vol. 41, No. 13* *Published online 9 May 2013*
doi:10.1093/nar/gkt358

Cell type specificity and structural determinants of IRES activity from the 5′ leaders of different HIV-1 transcripts

Terra-Dawn M. Plank[1], James T. Whitehurst[2] and Jeffrey S. Kieft[1,3,*]

[1]Department of Biochemistry and Molecular Genetics, [2]Department of Pharmacology and [3]Howard Hughes Medical Institute, University of Colorado Denver, School of Medicine, Aurora, Colorado, 80045, USA

Received March 18, 2013; Revised April 12, 2013; Accepted April 15, 2013

ABSTRACT

Internal ribosome entry site (IRES) RNAs are important regulators of gene expression, but their diverse molecular mechanisms remain partially understood. The HIV-1 gag transcript leader contains an IRES that may be a good model for understanding the function of many other IRESs. We investigated the possibility that this IRES' function is linked to both the structure of the RNA and its cellular environment. We find that in the context of a bicistronic reporter construct, HIV-1 gag IRES' activity is cell type-specific, with higher activity in T-cell culture systems that model the natural target cells for HIV-1 infection. This finding underscores how an IRES may be fine tuned to function in certain cells, perhaps owing to cell type-specific protein factors. Using RNA probing and mutagenesis, we demonstrate that the HIV-1 gag IRES does not use pre-folded RNA structure to drive function, a finding that gives insight into how conformationally dynamic IRESs operate. Furthermore, we find that a common exon drives IRES activity in a diverse set of alternatively spliced transcripts. We propose a mechanism in which a structurally plastic RNA element confers the ability to initiate translation internally, and activity from this common element is modulated by 3′ nucleotides added by alternative splicing.

INTRODUCTION

The HIV-1 genome is a multifunctional RNA serving as the template for proviral DNA synthesis, the primary transcript for a subset of >30 alternatively spliced transcripts, the template for translation of the viral packaging genes gag and gag-pol (the 'gag mRNA') and the RNA packaged into nascent viral particles [reviewed in (1)]. These diverse processes are largely organized and directed by the untranslated 5′ leader of the genomic RNA. The importance of the 5′ leader RNA to viral function is highlighted by its conservation (2), and this RNA provides a model system to study how a multifunctional leader operates in cells.

Of the diverse functions of the 5′ leader in the viral life cycle, its role in translation initiation remains only partially explored. Like cellular mRNAs, HIV-1 transcripts are produced in the nucleus and are capped and polyadenylated, and this presumably confers the ability to initiate translation through a canonical cap-dependent mechanism. However, the long and structured HIV-1 5′ leader is inhibitory to the ribosomal scanning used in cap-dependent translation initiation, suggesting that HIV-1 may also use an alternative initiation mechanism (3). Additionally, HIV-1 infection imposes several stresses on the cell that result in global inhibition of cap-dependent translation initiation (4–6). Therefore, it seems likely that HIV-1 has evolved alternate mechanisms of translation initiation, such as through a cap-independent internal process. In internal translation initiation, ribosomes are recruited to mRNAs independently of the cap and 5′ end through RNA elements known as internal ribosome entry sites (IRESs) (7). The mechanism for IRES-directed initiation varies; in some cases, ribosomes are recruited to the message directly without the need for protein factors. In other instances, a subset of the initiation factors are required and often additional IRES-trans acting factors (ITAFs; proteins not part of the canonical initiation machinery but used by an IRES) may be necessary. The role of diverse ITAFs in internal initiation is unclear, but

*To whom correspondence should be addressed. Tel: +1 303 724 3257; Fax: +1 303 724 3215; Email: Jeffrey.Kieft@ucdenver.edu

The authors wish it to be known that, in their opinion, the first two authors should be regarded as joint First Authors.

in some cases, the ITAFs may regulate internal initiation in a particular cell type or cellular state [reviewed in (8)]. A putative IRES in an HIV-1 transcript may have characteristics similar to cellular IRES RNAs, including ITAF requirements and the ability to initiate translation by both a cap-dependent and IRES-driven mechanism.

Studies investigating the mechanisms of translation initiation used by the HIV-1 gag mRNA leader (gag leader) [reviewed in (9)] have identified a cap-dependent pathway (10–13), an IRES-dependent pathway (14–16) or a combination of these mechanisms (17). A possible explanation for the identification of many different initiation strategies is that the experiments were performed in several different cell culture and cell-free systems, including rabbit reticulocyte lysate (RRL) (17), HeLa cells (14), xenopus oocytes (15) and Jurkat T-cells (18). The IRES may operate differently in these systems, but a direct side-by-side comparison of gag leader IRES activity in different cell types has not been presented.

In addition to the aforementioned genomic RNA/gag mRNA, HIV-1 produces >30 alternatively spliced transcripts encoding viral accessory proteins (19). The leader of each transcript contains a common 289 nucleotide non-coding exon at the 5′ end, with sequence unique to each transcript spliced onto the 3′ end of this common exon. The presence of a common element in the 5′ leaders of all HIV-1 transcripts and the fact that IRES activity has been observed for the gag leader suggests that all HIV-1 leaders may be capable of internal initiation. However, of these leaders, internal initiation has only been reported for the tat mRNA (20) in addition to the aforementioned gag mRNA (14). Thus, we do not have a complete understanding of the potential role of IRES-driven translation in the family of alternatively spliced mRNAs that are used to synthesize various HIV-1 proteins.

In this study, we considered the putative HIV-1 gag IRES as a model for examining how a multifunctional leader RNA, produced and processed in the nucleus, can operate as an IRES. We directly examined the cell type specificity of IRES activity from the HIV-1 gag leader, comparing the efficiency of internal translation initiation in diverse cell types. We find that this IRES' activity varies dramatically in different cell types, with robust activity in cell systems modeling the natural target cells for HIV-1 infection. Furthermore, we find that IRES activity in T-cells is largely conferred to the leader by a ~185 nucleotide element that is present in all viral transcripts. The functional role of RNA structure in this core IRES element differs from other well-studied viral IRESs in that a single pre-folded tertiary structure does not appear to be the primary driver of IRES function. Examining IRES activity in the context of several different HIV-1 leaders, we demonstrate for the first time that this element is functional in several alternatively spliced transcripts. We propose a mechanistic model for how a conformationally dynamic RNA can provide regulated IRES activity to a set of related mRNAs.

MATERIALS AND METHODS

Plasmid construction

IRES activity was studied using the dual-luciferase reporter vector pRL (21). The 5′UTRs of HIV-1 Gag, Nef, Vif, Vpr and Vpu were cloned into the EcoRI and NcoI sites of this construct by PCR amplification of plasmids containing 5′UTR sequences. For HIV-1 Gag constructs, 5′UTR sequences were amplified from pCrPV1.1 containing nucleotides 455–838 of HIV-1 NL4-3 (14), which corresponds to nucleotides 1–384 of the HIV-1 Gag mRNA. Plasmids containing the HIV-1 Nef, Vif, Vpr and Vpu 5′ UTR sequences were generated by Mr. Gene (Life Technologies) according to the predominant splicing patterns identified by Purcell *et al.* (19) and listed below. Nef: Splice donors (744, 6044), splice acceptors (5976, 8369), AUG start site (8787); Vif: Splice donor (743), splice acceptor (4913), AUG start site (5041); Vpr: Splice donor (743), splice acceptor (5390), AUG start site (5558); Vpu: Splice donor (743), splice acceptor (5976), AUG start site (6061). All nucleotide numbering is relative to pNL4-3. The dual-luciferase reporter vector pRL containing the β-Globin or Tau 5′ leader insert was a gift from the Krushel laboratory, and the hepatitis C virus (HCV) IRES-containing reporter plasmid has been described previously (22).

HIV-1 Gag 5′UTR deletion mutants were generated by amplifying fragments of the 5′UTR and inserting into the EcoR1 and Nco1 sites of the dual-luciferase vector. HIV-1 Gag apex mutants and helix disruptions were generated by a QuickChange PCR reaction using Gag 1-384 dual-luciferase vector as a template and the primer pairs listed in Supplementary Table S1. HIV-1 Gag mutations dimerization initiation site (DIS)-L1-4, primer binding site (PBS)-H1-2 and packaging signal (PSI)-H1-2 were created using PCR amplification with mutation-encoding primers to produce two overlapping fragments of the 5′ UTR harboring the desired sequence changes. The fragments were annealed, extended and amplified by a second PCR reaction with common primers before subcloning into the dual luciferase vectors between the EcoRI and NcoI sites. Common primers: forward 5′gcgagtgaattcggtctctctggttagaccag3′, reverse 5′gcgatccatggcccatttatc3′. Mutagenesis primers are listed in Supplementary Table S1.

The HIV-1 gag 1-384 linker and HIV-1 gag 1-348 linker constructs were made by PCR amplification of gag 1–384 or gag 1–348, adding 5′ ggtggaggaggttctggaggcggtggaagtggtggcggaggtagc 3′ sequence on the 3′ end of the reverse primer. PCR fragments were cloned into the EcoRI and NcoI sites of the dual luciferase reporter plasmids.

Monocistronic constructs were generated by PCR amplification of nucleotides 336–384 + firefly luciferase (FLUC) sequence or nucleotides 348–384 + FLUC and inserted into the EcoRI and XhoI sites of pcDNA3. The FLUC AUG was then deleted by a quick-change reaction using the following primer pairs: gag 336–384 (Gag 384 Luc AUG del F Gaattagataaatgggccgaagacgccaaaaacataaagaaaggc Gag 384 Luc AUG del R gtttttggcgtcttcggcccatttatctaattctccCCCGC), gag 336–348 (Gag 348 Luc AUG del F GGAATTCatgggtgcgagagccgaagacg

Table 1. Raw luciferase values from transfections

Cell type, IRES	Ratio FLUC/RLUC	RLUC (RLUs)	FLUC (RLUs)
RRL			
HCV	0.342 ± 0.011	1.74E + 07	5.94E + 06
HIV-1 gag	0.011 ± 0.002	1.74E + 07	1.90E + 05
β-Globin	0.017 ± 0.001	1.77E + 07	3.01E + 05
Hek 293			
HCV	not tested		
HIV-1 gag	0.052 ± 0.010	3.85E + 04	1.97E + 03
β-Globin	0.044 ± 0.003	7.63E + 04	3.41E + 03
HeLa			
HCV	0.814 ± 0.031	1.40E + 05	1.14E + 05
HIV-1 gag	0.028 ± 0.000	4.08E + 05	1.13E + 04
β-Globin	0.057 ± 0.001	2.39E + 05	1.37E + 04
Jurkat			
HCV	0.367 ± 0.031	1.04E + 05	3.68E + 04
HIV-1 gag	0.145 ± 0.008	2.60E + 05	3.76E + 04
β-Globin	0.009 ± 0.001	1.21E + 05	1.09E + 03
CEM-C1			
HCV	0.514 ± 0.111	1.27E + 04	6.53E + 03
HIV-1 gag	0.277 ± 0.012	5.60E + 04	1.53E + 04
β-Globin	0.079 ± 0.003	3.50E + 04	1.71E + 03
HSB-2			
HCV	1.824 ± 0.117	1.60E + 05	2.86E + 05
HIV-1 gag	1.496 ± 0.029	5.71E + 05	8.53E + 05
β-Globin	0.042 ± 0.002	1.25E + 05	5.26E + 03
HPB-ALL			
HCV	0.313 ± 0.029	1.32E + 05	4.34E + 05
HIV-1 gag	0.563 ± 0.008	3.88E + 05	2.20E + 05
β-Globin	0.031 ± 0.001	1.03E + 05	3.16E + 03
THP-1			
HCV	0.046 ± 0.003	2.72E + 06	1.24E + 05
HIV-1 gag	0.064 ± 0.006	2.16E + 06	1.35E + 05
β-Globin	0.005 ± 0.001	3.06E + 06	1.47E + 04

Errors for raw LUC measurements are not shown; values for the FLUC/RLUC ratio are the average of at least three independent experiments ± SEM.

ccaaaaacataaagaaaggc Gag 348 Luc AUG del R gtt tttggcgtcttcggctctcgcacccatGAATTCCAGCACACTGG).

Plasmids used for the hydroxyl radical probing experiments were generated by PCR amplification of nucleotides 1–336 of HIV-1 gag, adding a 5′ hammerhead and a 3′ hepatitis delta ribozyme under the control of a T7 promoter. This insert was cloned into the EcoR1 and BamHI sites of a pUC19 vector. An identical plasmid containing the HCV IRES in place of the HIV-1 gag leader is described previously (23).

All plasmids used in this study were verified by sequencing.

In vitro transcription

RNA for *in vitro* translation was synthesized using the MegaScript Kit (Ambion), according to the manufacturer's protocol. Dual-luciferase template DNA was generated by linearizing pRL plasmid DNA with BamHI. Monocistronic template DNA was generated by linearizing pcDNA3 with XhoI. *In vitro* transcriptions were incubated at 37°C for 2.5 h. The template DNA was digested with DNase I, and RNA was extracted with Tri-Reagent (Sigma), followed by isoproponal precipitation, followed by ethanol precipitation. RNA was resuspended in 20 µl of nuclease free water. Template DNA used to generate RNA constructs in hydroxyl radical probing experiments was amplified from the pUC19 plasmid with M13-Forward and M13-Reverse primers. The resulting PCR product contains a T7 promoter followed by a 5′ hammerhead ribozyme, the template of interest and a 3′ hepatitis delta ribozyme. DNA templates were transcribed by T7 polymerase for 2 h at 37°C and then were placed at 65°C for 5 min. The reaction was precipitated by adding 2 volumes of ice-cold 100% ethanol, and the RNA was collected by centrifugation. The resulting RNA was purified by gel electrophoresis on an 8% denaturing polyacrylamide gel. The band containing the RNA was visualized by ultraviolet (UV)-shadowing, excised from the gel, crushed and allowed to elute into RNase-free water overnight. The gel pieces were filtered out of the solution using a 0.22-µm filter (Millipore). The RNA then was concentrated using a centrifugal filter with a 50 000 molecular weight cutoff (Amicon). Purity was assessed by polyacrylamide gel electrophoresis. RNA concentration was determined spectrophotometrically (Nanodrop), and integrity was monitored by polyacrylamide gel electrophoresis.

In vitro translation assays, ^{35}S-met incorporation and SDS–PAGE

In vitro translation reactions were performed using the nuclease treated RRL system (Promega) according to the manufacturer's protocol. Briefly, 1 µg of RNA was used in a reaction containing 70% lysate, 10 µM amino acids (minus Leu), 10 µM amino acids (minus Met), 0.5 mM $MgCl_2$ and 1 µl of RNASE inhibitor, in a final reaction volume of 25 µl. In all, ^{35}S incorporation assays were performed as described earlier in the text but using 20 µM amino acids (minus Met), supplemented with 1 µl of ^{35}S-met (1200 Ci/mmol at 10 mCi/ml, Perkin Elmer). Reactions were incubated at 30°C for 90 min. In all, 10 µl of the reaction was diluted in 90 µl of 1 x Passive Lysis Buffer (Promega) and used for a luciferase assay, and 5 µl of the reaction was used to run on a 10% SDS–PAGE gel. ^{35}S-met incorporation was quantitated by autoradiography using ImageQuant.

Cell culture and transfections

HeLa and HEK 293 cells were cultured in Dulbecco's modified Eagle's medium supplemented with 10% FBS at 37°C in a 5% CO_2 atmosphere. Twenty-four hours before transfection, cells were plated at 60% confluency in a 24-well dish. HeLa cells were transfected with 250 ng of DNA, 0.25 µl of Plus reagent and 0.5 µl of Lipofectamine LTX, according to the manufacturer's protocol (Invitrogen). HEK 293 cells were transfected with 250 ng of DNA and 2 µl of Lipofectamine 2000, according to the manufacturer's protocol (Invitrogen). Twenty-four hours post-transfection, cells were harvested with 100 µl 1x Passive Lysis Buffer (Promega). Samples were either stored at −20°C or assayed directly for luciferase activity.

Jurkat cells (ATCC #TIB-152) were maintained in RPMI 1640 supplemented with 10% FBS at 37°C in a

5% CO_2 atmosphere. Cells were transfected with Lipofectamine LTX and Plus reagent (Invitrogen) at a density of 100 000 cells per well in a 24-well dish. Cells were transfected with 1 μg of plasmid DNA, 1 μl of Plus reagent and 1 μl of Lipofectamine LTX, according to the manufacturer's protocol. Cells were transfected in standard media containing 4 μg/ml Concanavalin A (Sigma). Twenty-four hours post-transfection, cells were harvested as described earlier in the text for HeLa cells.

CEM-C1 (ATCC # CRL-2265), HSB-2 (DSMZ #ACC 435), HPB-ALL (DSMZ #ACC 483) and THP-1 (ATTC # TIB-202) cells were maintained in RPMI 1640 supplemented with 10% FBS at 37°C in a 5% CO_2 atmosphere. Cells were transfected using the Neon electroporation system (Invitrogen). Briefly, 200 000 cells in buffer R were electroporated in 10 μl tips with 1 μg of plasmid and plated into 500 μl of standard media in a 24-well dish. The electroporation parameters varied by cell line (CEM-C1: 1175 V, 30 mA, 2 pulses, HSB-2: 1150 V, 30 mA, 2 pulses, HPB-ALL: 1600 V, 10 mA, 3 pulses, THP-1 1400 V 20 mA 2 pulses). Twenty-four hours post-transfection, cells were harvested as described earlier in the text for HeLa cells. For THP-1 differentiation, THP-1 cells were electroporated as described earlier in the text, but plated into 500 μl of media supplemented with 2 nM phorbal myristal acetate (PMA, Sigma). On differentiation (generally 24–36 h post-transfection), cells were harvested.

Luciferase assays

Lysates were analyzed for luciferase activity using the dual-luciferase system (Promega). Lysates were analyzed in a 96-well plate format on a Glomax 96-well plate reader. A total of 20–50 μl lysate was analyzed with 100 μl of LAR II reagent and 100 μl 1 × Stop N Glo reagent. Results are reported as the average measurement obtained from at least three independent transfections, with each construct transfected in triplicate.

Hydroxyl radical probing

RNA was 5′ end labeled using T4 Polynucleotide Kinase (PNK, NEB) and [γ -^{32}P] ATP (6000 Ci/mmol, Perkin Elmer). The labeling reaction was conducted in a 20 μl volume containing 20 μg of RNA, 20 Units T4 PNK, 0.15 mCi P32 [γ -^{32}P] ATP in 1 × PNK buffer (NEB). The RNA was purifed on a 10% denaturing polyacrylamide gel and eluted in 250 μl of buffer (500 mM NaOAc at pH 5. 2, 0. 1% SDS). RNAs were ethanol precipitated and resuspended in Diethyl pyrocarbonate (DEPC)-treated water at a concentration of 200 000 cpm/μl. Hydroxyl radical probing and the generation of RNase T1 and hydrolysis ladders were performed as described previously (23,24). Briefly, 200 000 cpm of end labeled RNA was heat cooled and then placed in 30 mM Hepes-NaOH (pH 7. 5), 0 or 10 mM $MgCl_2$ and 0.1 mg/ml tRNA and incubated at 37°C for 20 min. Cleavage reactions were initiated by sequentially adding the following: Fe(II)-EDTA solution (2 mM sodium EDTA, 1 mM ferrous ammonium sulfate), 5 mM sodium ascorbate and hydrogen peroxide at either 0.15% (for HCV) or 0.05% final concentration (for HIV-1). Cleavage reactions were conducted at 37°C for 2 min and quenched with the addition of 10 mM thiourea and one reaction volume of 9 M urea/1 mM EDTA. Cleavage products were resolved on a 10% sequencing denaturing polyacrylamide gel (1 × TBE, 7 M urea, 29:1 acrylamide:bis-acrylamide) and visualized with a phosphorimager. Cleavage products were quantitated using ImageQuant and analyzed using Excel.

Reverse transcription and quantitative PCR

Twenty-four hours post-transfection, total RNA was harvested immediately from 5×10^6 Jurkat cells using Tri Reagent (Sigma) as described by the manufacturer's protocol. RNA pellets were resuspended in 30 μl of RNASE-free water, treated with DNASE (DNA-free, Ambion) according to the manufacturer's protocol and either used immediately in an RT reaction or stored at −80°C for no longer than 1 week. RNA concentration was quantified spectrophotometrically by A260 values (Nanodrop; Thermo Scientific), purity was assessed by A260:A280 ratios (2.0) and integrity was monitored by agarose gel electrophoresis. All extractions yielded RNA concentrations of ∼200 ng/μl. cDNA synthesis (iscript, BioRad #170-8891) was performed in triplicate with 100 ng RNA in a 20 μl of reaction volume, according to the manufacturer's protocol.

Real-time PCR was carried out in 10 μl of reaction volume using 4 μl of a 1:80 dilution of cDNA, 100 nM of each primer and SyberGreen (Express Syber Green ER, Invitrogen) according to the manufacturer's protocol. Quantitative PCR (qPCR) was conducted in a 384-well format on the Roche LC-480 (Roche Applied Science) with the following cycling parameters: Denaturation was for 5 min at 95°C followed by 50 cycles of 15 s 95°C, 20 s 60°C, 20 s 72°C. Each sample was run in duplicate. No-template controls were run for each pair of primers, and minus-RT reactions were also performed. Primer sets were designed using Roche Light Cycler Probe Design version 2.0 with melting temperatures between 55°C and 62°C. PCR product size ranged from 150 to 300 base pairs. All primer sets used gave single melting point curves that were monitored at the end of each run. All primer pairs used for analysis had amplification efficiencies between 1.8 and 2.2. Pairs: RLUC 1: (Forward: 5′GGAAACCATGTTGC CATC3′ Reverse: 5′TTCCTAACAATTTGTACAACGT CAG3′) RLUC2: (Forward: 5′ACCTGACGTTGTACA AATTGTTA3 ′ Reverse: 5′ AGGTGCATCTTCTTGCG 3′) RLUC3: (Forward: 5′ GTGCTTGTTTGGCATTTC ATTA3′ Reverse: 5′ATGCTGCAAATTCTTCTGG3′) FLUC 1 (Forward 5′CATGAACTCCTCTGGATCTA C3′ Reverse 5′GTGATGGAATGGAACAACACT3′) FLUC 2 (Forward 5′TGGGCTGAATACAAATCA CAGA3′ Reverse 5′AACGAACACCACGGTAG3′) FL UC 3 Forward 5′ GGATTACAAGATTCAAAGTGC G3′ Reverse 5′ ATGGAACAACTTTACCGACC3′).

RNA levels were quantified relative to an eight-point dilution series containing sheared genomic DNA titrated with pRL plasmid DNA (1–100 ng of genomic DNA and 0.005–0.5 pg plasmid DNA) using the Absolute Quantification 2nd Derivative Maximum method with

Lightcycler 480 1.2 software (Roche). RNA levels were quantified in this manner with three different primers targeting each gene, and the values from each primer pair were averaged and normalized to renilla luciferase (RLUC). Three independent qPCR experiments were performed from three independent transfections, and results are displayed as the average relative FLUC and RLUC values from these experiments. Cq values from the no-template control reactions, or from the minus-RT reactions were either not detected or were at least 5 degrees greater than the highest Cq produced in the standard curve. All Cq values used for analysis were within the linear range of the standard curve.

RESULTS

Internal translation initiation from the HIV-1 gag leader is cell type specific

We hypothesized that internal translation initiation from the 5′ leader of the gag transcript (hereafter referred to as the gag leader) may operate at variable efficiency in different cells. To explore this, we used a plasmid encoding a dual-luciferase reporter mRNA in which the gag leader sequence was inserted between an upstream RLUC (cap-dependent initiation) and a downstream FLUC (IRES-dependent initiation) (Figure 1A). Transfection of cells with this DNA construct results in production of a capped and poly-adenylated dicistronic mRNA. Although this transcript has the gag leader in a context that differs from its natural position at the 5′ end, we chose this dual-luciferase system to exclusively measure cap-independent initiation from the leader un-confounded by cap-dependent initiation. The IRES activity is defined as the ratio FLUC/RLUC relative light units (RLUs); the RLUC levels are an internal control for transfection efficiency and cap-dependent translation levels.

We first tested an RNA sequence comprising nucleotides (nts) 1–384 of the gag transcript RNA; this contains the entire 5′ leader plus an additional 46 nts of the gag open reading frame (ORF). We included this part of the gag ORF for several reasons: first, this places the ORF in an authentic structural and sequence context, and portions of ORFs have been shown to affect the activity of other IRESs. Second, we wanted to directly compare our results to previous studies that included this region (14,16,18). Although a second IRES has been identified in the gag ORF(16), the hypothesized core region of this second IRES is downstream of the regions we include (25), eliminating potential complications owing to the action of two IRESs. We tested translation initiation from 1 to 384 nt in RRL, HEK 293 cells, HeLa cells and Jurkat T-cells. In RRL, HEK 293 and HeLa cells, IRES activity was comparable with the negative control β-globin construct, indicating that 1–384 nt of the gag leader is an inefficient IRES in these cell types and lysates (Figure 1B).

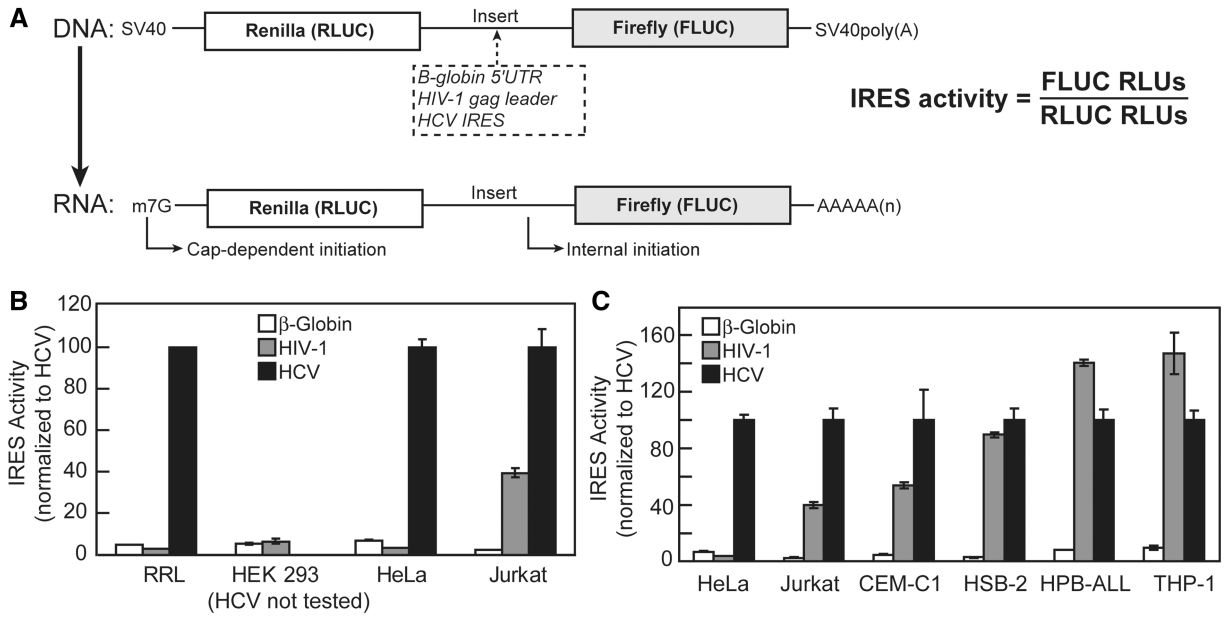

Figure 1. Internal translation initiation from the HIV-1 gag 5′ leader is cell type specific. (**A**) Diagram of reporter constructs. The 5′ UTR DNA sequences from β-globin, HIV-1 gag (1–384 nts), or HCV mRNAs were inserted between two luciferase genes. Transcription from this DNA construct in cells is initiated from a single SV40 promoter and produces a capped and poly-adenylated dicistronic message. Translation of the upstream cistron (renilla luciferase, RLUC) is cap dependent, whereas translation of the downstream cistron (FLUC) occurs cap independently. IRES activity is defined as the ratio of FLUC to RLUC light production (RLUs). (**B**) RRL was treated with *in vitro* transcribed dicistronic RNA, and IRES activity was measured. HEK 293, HeLa and Jurkat cells were transfected with distronic DNA constructs and IRES activity was measured. HCV was not tested in HEK 293 cells, β-globin and HIV-1 gag measurements in these cells were normalized to HCV in HeLa. (**C**) T-cells (CEM-C1, HSB-2, HPB-ALL) and monocytes (THP-1) were transfected with dicistronic DNA constructs, and IRES activity was measured. Results are displayed as the averages of at least three independent experiments plus the standard error of the mean (SEM) and are normalized to the HCV IRES' activity (values set at 100) within each cell type. All readings were within the linear detection range of the luminometer. Raw RLU measurements are presented in Table 1.

However, expression of the reporter in Jurkat T-cells resulted in IRES activity 15-fold greater than the negative control construct and 2.5-fold less than the activity of the positive control HCV IRES. These data preliminarily indicated that the level of IRES activity from the gag leader is cell-type dependent, with higher activity in Jurkat T-cells.

Apparently high IRES activity may be due to the generation of monocistronic FLUC mRNAs from cryptic splicing or promoter activity, rather than from IRES activity in a full dual-luciferase mRNA. A previous study performed in Jurkat cells with the HIV-1 gag leader IRES used an shRNA-based approach to eliminate these possibilities (18), we took two additional approaches. We first measured RLUC and FLUC mRNA levels produced in the cell by quantitative reverse transcriptase PCR (qRT-PCR) using primer pairs that span each of the luciferase ORFs. A positive control construct containing a known cryptic promoter and/or splice site [TAU 5′UTR, (26)] produced more FLUC than RLUC mRNA, whereas an authentic IRES without a cryptic promoter or splice site (Encephalomyocarditis virus (EMCV) IRES) produced equal amounts of the two. Like the authentic EMCV IRES, the gag leader produced equal levels of FLUC and RLUC RNA, strongly suggesting there are no cryptic events leading to the production of functional monocistronic FLUC mRNA (Supplementary Figure S1). Furthermore, because we used multiple primer pairs, each ORF was surveyed in several places, strongly suggesting that each ORF was intact. These results indicate that full length FLUC- and RLUC-encoding mRNAs are being produced in equal amounts from the gag containing DNA, strongly arguing against the presence of cryptic splicing or promotor activity. However, an event in which only the IRES was spliced out, resulting in a chimeric RLUC–FLUC message with no intervening sequence and identical amounts of each reporter mRNA, would not be detected by this qPCR approach (Supplementary Figure S2). Therefore, we performed RT-PCR to detect the sizes of FLUC-containing RNA species produced in the cell using a primer pair upstream of the RLUC ORF and within the FLUC ORF. Analysis of RNA after transient transfection with the plasmid encoding the dual-luciferase gag leader construct resulted in a single PCR product of 1700 bp (Supplementary Figure S2), corresponding to the expected product size of dual-cistronic RNA. Use of a second primer within the RLUC ORF yielded a single sized product of 1455 bp, again matching the size of the product expected from full-length intact mRNA. If aberrant splicing were occurring, smaller PCR products would be observed, particularly products of ~1316 and 1071 bp would be detected if just the putative IRES were spliced out. As smaller products were not observed, these data strongly suggest that cryptic processing events are not contributing to apparent IRES activity.

To test whether apparent IRES activity was due to read-through of ribosomes from the RLUC ORF to the FLUC ORF, we inserted a defective EMCV IRES sequence known to inhibit read-through and re-initiation upstream of the gag leader sequence (27,28). This did not decrease apparent IRES activity, indicating that initiation of the downstream cistron occurs independently of the upstream cistron (Supplementary Figure S3). Finally, it has been reported that the HIV-1 IRES is more active in the G2/M stage of the cell cycle when cap-dependent translation is depressed; if Jurkat cells are spending more time in G2/M than are HeLa cells, the increase in the FLUC/RLUC ratio in Jurkat cells might be due to a decrease in cap-dependent translation rather than robust IRES activity. However, cell cycle analysis of Jurkat and HeLa cells indicated the same relative populations of cells in each stage; thus, changes in apparent IRES activity are not a result of cell cycle-dependent differences in cap-dependent translation (Supplementary Figure S4). Taken together, these and published results strongly argue for authentic and robust IRES activity from the HIV-1 leader in Jurkat cells.

The higher gag leader IRES activity in Jurkat T-cells compared with HeLa and HEK 293 cells suggested that the IRES might also have robust activity in other T-cell lines. To test this, we transfected three additional T-cell lines (CEM-C1, HSB-2 and HPB-ALL) with the dual-luciferase construct and measured IRES activity (Figure 1C). In all T-cell lines tested, IRES activity from the gag leader was robust; in some cases higher than that produced by the HCV IRES. We also tested HIV-1 gag IRES activity in another target cell type, a monocytic cell line (THP-1) and observed robust levels of IRES activity as compared with the negative control construct. Although we cannot eliminate the possibility that changes in RLUC production (cap-dependent translation) lead to apparent changes in IRES activity (Table 1), these data suggest a trend in which IRES activity from the gag leader is higher in cell types that are natural targets for HIV-1 than in those that are not. We therefore selected Jurkat T-cells as a good model to further explore gag leader IRES activity.

The core HIV-1 gag IRES element in T-cells contains the PBS, DIS, major splice donor site and PSI domains

The markedly higher level of HIV-1 gag IRES activity in T-cells raises the question of whether the IRES RNA sequence and structural determinants of function differ in these cells compared with those within HeLa cells. We therefore created a series of constructs in which the IRES was systematically truncated from the 5′ and 3′ ends and assayed for activity in Jurkat cells using the dual-luciferase reporter system (Figure 2A). Some of these deletion constructs were purposefully made to match constructs previously tested in HeLa cells to allow direct comparison, whereas others had not been previously tested.

We first examined 5′ and 3′ truncations separately. Truncating from the 5′ end (Figure 2B), deletion of the trans-activating region and Poly(A) domains (57–384 and 104–384, respectively) modestly stimulated IRES activity. Truncation to partially remove the 5′ end of the PBS domain (132–384) resulted in an additional increase, whereas further truncation to 179 nt (179–384) caused a decrease, indicating that regions between 132 and 179 nt promote IRES function. This result differs from a

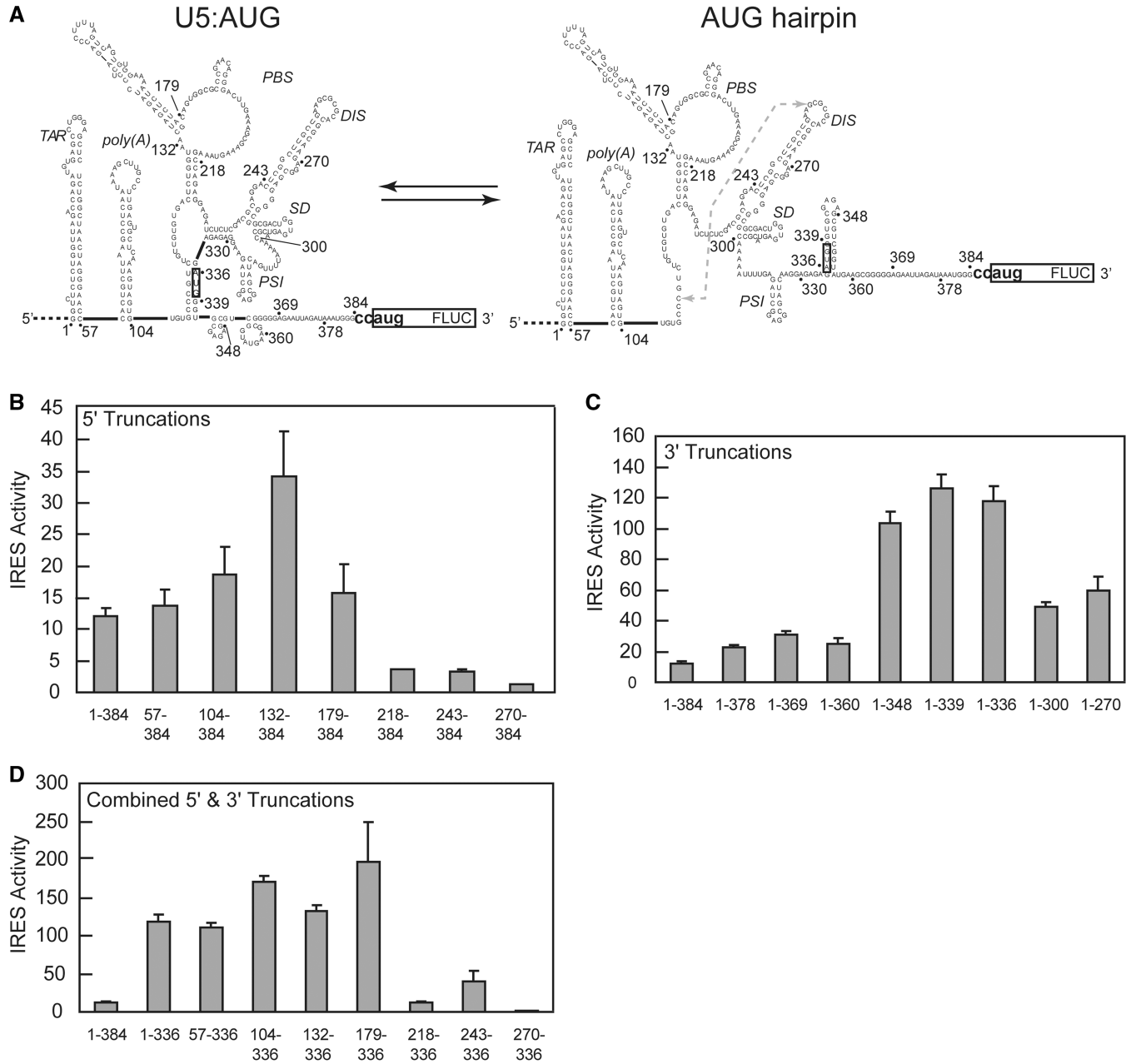

Figure 2. Defining the IRES element by 5′ and 3′ truncations. (**A**) Secondary structure models of the HIV-1 gag 5′ leader, 1–384 nts. Left: form proposed to be translation repressed, but in which the DIS is available to dimerize. Right: form proposed to be translationally competent, where the DIS is paired with the U5 region (gray dashed arrow) (29,30). The authentic initiator AUG is boxed, and the position of the FLUC start codon AUG and ORF is shown. The FLUC AUG is contained within the NcoI cloning site (ccaugg) and is depicted by bold nucleotides upstream and within the FLUC ORF. Nucleotide positions of 5′ and 3′ deletion mutants are diagrammed. The leader regulatory domains are indicated: the Trans-activating region (TAR), the polyadenylation signal [poly (A)], the PBS, the DIS, the SDand the PSI (**B**, **C** and **D**). IRES activity was measured from Jurkat cells transfected with dual-luciferase DNA construct containing HIV-1 gag 5′ leader truncation mutants. Construct numbering indicates the nucleotide position of the 5′ and 3′ ends of the construct, with the 3′ nucleotide position preceding the NcoI site. Results are displayed as the averages of at least three independent transfections, plus SEM and are normalized to the β-globin construct that was set at 1.

previous study showing deletion of 132–179 nts resulted in an increase an activity (18) and may be accounted for by the differences in approach, i.e internal deletions, versus truncations. Further deletion of the DIS, major splice donor site (SD) and PSI domains led to substantial decreases in IRES activity (218–384, 243–384 and 270–384). From the 3′ end, truncation of the IRES from 384 to 360 nt resulted in relatively small changes in activity (<2-fold), whereas truncation to 348 resulted in an 8-fold increase in IRES activity (compare 1–384 to 1–348, Figure 2C). As the 348 truncation removes 36 nt of gag ORF (from 384 to 348 nt), this result suggests that regions of the gag ORF inhibit IRES function. Further truncation from the 3′ end to 336 nt resulted in no

additional change in IRES activity, but deletion of the PSI and SD domains caused a decrease in IRES activity (constructs 1–300 and 1–270) relative to construct 1–336.

Having truncated from the 5′ and 3′ ends individually, we then truncated the 3′ end of the IRES back to nt 336 (removing the gag ORF inhibitory region) and tested several 5′ truncations in this context (Figure 2D). As expected, without the gag ORF IRES activity increased, with construct 179–336 containing the highest activity of all the truncation mutants tested. Overall, the 5′ truncations show a pattern similar to what is observed when the gag ORF is included with some difference between 104 and 179 nts and 218–243 nts (compare Figure 2B and D). Additionally, we observe an increase in IRES activity when we truncate to 104 nt, whereas a decrease in activity was observed in a study performed in HeLa cells (14). Taken together, these results show that truncations from both the 5′ and 3′ ends increase IRES activity, suggesting that there are RNA sequences/structures in these regions that modulate activity of a central 'core' region that is the primary driver of IRES activity. Strict delineation of the core region is difficult, but our data suggest that in Jurkat cells, this region is primarily contained between 179 and 336 nts, which includes part of the PBS, DIS, SD and PSI domains. Notably, there is an inhibitory effect when RNA downstream of the core elements (i.e. part of the gag ORF) is included.

Gag ORF sequences inhibit IRES activity

Inhibition of HIV-1 gag IRES activity by the gag ORF is well documented (14,16,31,32), but the mechanism remains elusive. This motivated us to explore the cause of the inhibition of gag IRES activity when 336–384 nts are present. The first possibility we considered is that the enzymatic activity of the FLUC reporter is altered by additional amino acids (aa) on its N-terminus when part of the gag ORF is present. If true, measurements of FLUC activity would not accurately reflect the amount of protein produced, and the observed inhibitory effect of the gag ORF would not be due to *bona fide* changes in translation initiation levels. The second possibility is the previously posited explanation that formation of RNA secondary structure inhibits internal initiation when the gag ORF is present (14).

To explore the possibility that the amino acids added to the N-terminus reduces FLUC enzymatic activity, we simultaneously measured, in an *in vitro* reaction: (i) the enzymatic activity of the FLUC and (ii) protein amounts produced. To do this, we used two monocistronic RNAs in which parts of the gag ORF sequence were added to the 5′ end of the FLUC ORF, and the FLUC start codon was deleted to prevent initiation from that location (Figure 3A). We also included a 47 nt non-IRES control UTR on the 5′ end of the constructs. The two constructs contain 336–384 nt (336–384 + FLUC) or 336–348 nt (336–348 + FLUC) of the gag ORF fused to the FLUC ORF. Translation of these RNAs produces the same proteins generated by constructs 1–384 and 1–348 of Figure 2C, namely, FLUC protein with 17 or 5 aa added to the N-terminus, respectively. These RNAs were made, purified *in vitro* and translated in RRL. Protein production was directly quantitated by S^{35}-methionine incorporation visualized by SDS–PAGE and compared with FLUC activity from the same *in vitro* reactions. The ratio of these two measurements is an estimate of the FLUC activity/unit protein. We found that the 336–384 + FLUC (+17 aa) had a 35% decrease in relative luciferase activity compared with the 336–348 + FLUC (+5 aa) construct, suggesting that in this system, the addition of some gag protein sequence to the N-terminus of FLUC partially inhibits luciferase activity (Figure 3B). However, the 336–384 + FLUC (+17 aa) consistently had a 70% reduction in protein levels as compared with the 348 + FLUC (+5 aa) construct, indicating a defect in protein synthesis in addition to a decrease in enzymatic activity. We also used a second approach to monitor the effect of the gag amino acids on FLUC activity. We made a dual-luciferase construct containing a sequence encoding a flexible $(Gly\text{-}Gly\text{-}Gly\text{-}Gly\text{-}Ser)_3$ linker between the gag amino acids and the FLUC in both the gag 1–384 and gag 1–348 constructs and measured activity in Jurkat cells (Figure 3C). Insertion of the linker did not increase IRES activity as compared with the no linker counterpart (Figure 3D), suggesting that in cells the added amino acids are not inhibiting the activity of FLUC. We also considered the possibility that the added amino acids affect luciferase stability. We measured luciferase protein half-lives from the gag 1–336, 1–348 and 1–384 constructs and determined that they were all ~3 h (Supplementary Figure S5). In summary, although the addition of N-terminal amino acids on the FLUC reporter causes some loss in enzymatic activity (in RRL), direct quantitation of FLUC protein production by ^{35}S incorporation shows an even greater decrease in protein production. Based on this, and the fact that inclusion of a linker between the added amino acids and the reporter protein did not alter activity in cells (Figure 3D), we conclude that the decrease in apparent IRES activity owing to the ORF is caused mostly by a decrease in protein synthesis, perhaps caused by RNA structure.

Considering RNA structure as the source of the gag ORF inhibition effect, the secondary structure models in Figure 2A provide some insight (29). In the U5:AUG model, the initiator AUG is base paired to upstream sequence, which may make it less accessible to the translation machinery, decreasing IRES activity. Evidence for this is found in the activity of the aforementioned truncation constructs (Figure 2B and D). Specifically, in the context of the gag ORF, truncating the 5′ end from 104 to 132 (RNAs 104–384 and 132–384) would eliminate these potential base pairs to the AUG, and this would be predicted to increase activity, as we observe. This truncation would also drive formation of the 'AUG hairpin' secondary structure state that is proposed to be more translationally active (Figure 2A) (29). However, when the gag ORF is not present (the RNAs that end at 336), the sequence of RNA that contains the AUG is replaced with an Nco I restriction site (ccaugg), disrupting putative base pairing of the AUG codon in both the 'U5:AUG' and 'AUG hairpin' states. Hence, truncation from 104 to 132 in this context (104–336 and 132–336) would not

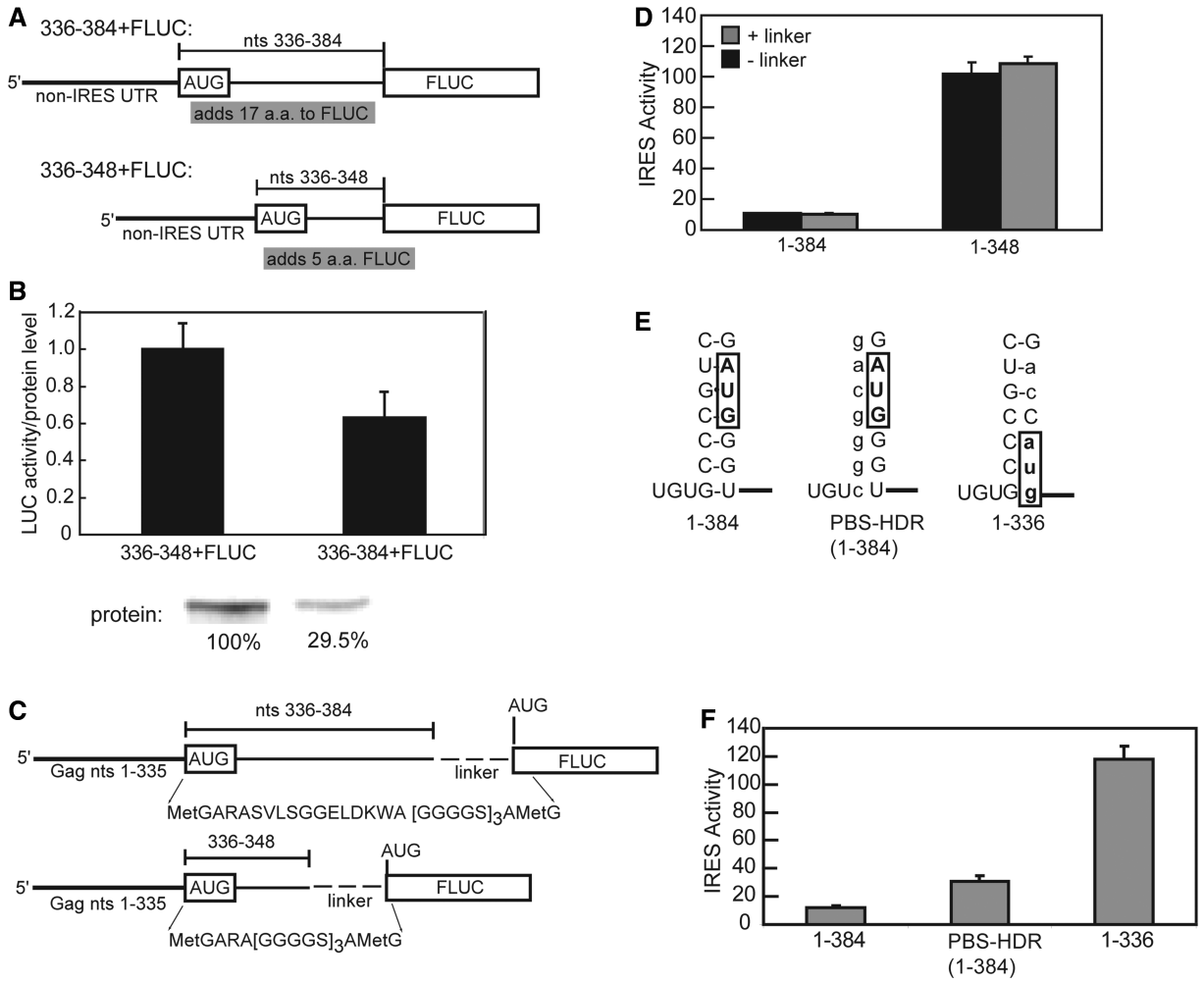

Figure 3. Regions of the gag ORF are inhibitory to IRES activity. (**A**) Diagrams of monocistronic FLUC RNA constructs containing regions of the gag ORF. The location of the initiator AUG is boxed. A 47-nt non-IRES control UTR was included on the 5′ end. (**B**) RNA constructs of panel A were used in an *in vitro* translation assay containing ^{35}S-methionine (gel under graph). Luciferase protein production was measured by ^{35}S incorporation, and FLUC was measured by a luciferase assay. Results are displayed as the ratio of FLUC relative to protein amounts and are normalized to the gag 336-348 construct. Results are displayed as the averages of three independent experiments, plus SEM. (**C**) Dual luciferase constructs were modified to contain a flexible $[GGGGS]_3$ linker (dashed lines) between the gag ORF and the FLUC AUG. The amino acids fused to the FLUC are shown below the construct. (**D**) Dual luciferase constructs with and without the linker were transfected into Jurkat cells, and IRES activity was monitored. The experiment was performed three independent times, and the results varied by <1%. Results are displayed as the average of a single experiment performed in triplicate, plus the SEM and normalized to β-globin, which was set at 1. (**E**) Secondary structure diagram depicting the nucleotide sequence contained within the PBS-AUG stem loop (1–384), and the altered nucleotides in the 1–336 construct, and the helix disruption mutant (PBS H1 DR). Wild-type nucleotides are capitalized, mutated nucleotides are lower case and the position of the initiator AUG is boxed. (**F**) Constructs were transfected into Jurkat cells, and IRES activity was measured. Results are displayed as the averages of at least three independent transfections, plus SEM and normalized to β-globin, which was set at 1.

remove any more base pairs, and thus no increase in activity is expected, as we observe.

Given that the presence of the gag ORF could promote base pair in both the 'U5:AUG' and 'AUG hairpin' configurations (Figure 2A) (29), we considered each possibility separately. We first generated a full-length (1–384) construct that was mutated to disrupt potential base pairing of the AUG within the 'U5:AUG' model (Figure 3E; PBS-HDR). In Jurkat cells, this mutant has 2-fold higher IRES activity compared with WT 1–384 (Figure 3F), similar to that observed when the helix is disrupted by truncation from the 5′ end (compare 104–384 and 132–384, Figure 2B). However, the PBS-HDR mutation did not raise IRES activity to the levels observed when the ORF is deleted and base pairing is disrupted (compare PBS-HDR and 1–336, Figure 3F). This result suggests that base pairing of the start AUG to upstream regions within the 'U5:AUG' structure is not entirely responsible for the inhibition caused by the gag ORF. Considering the 'Hairpin' structure, the AUG is base paired with nucleotides 353–356 of the gag ORF, rather than with the upstream 111–113 nts (Figure 2A). If the 'Hairpin' model is being adopted, we would expect truncation from 360 to 348 nt to disrupt this pairing and increase IRES activity; this is what we observe (Figure 2C). It is also possible that shifting of the location of the AUG (caused by our cloning) alters IRES activity; if this were the case, we would see low

IRES activity from constructs 1–348 and 1–339, as the AUG is in the same location as in 1–384; however, we see the opposite (Figure 2C).Overall, our data support AUG base pairing as a mechanism for the inhibition of IRES activity imposed by the gag ORF and suggest that this mechanism is operating in the 'Hairpin', rather than the 'U5:AUG' structure, consistent with the notion that the former is the translationally active form (29).

Stem-loop elements in the HIV-1 gag IRES perform different roles than in other viral IRESs

Having seen that secondary structure could play a role in altering IRES activity, we now explored the role of specific structural elements in IRES activity. We made mutants based on the observation that the gag IRES contains several stem-loop structures; this is significant because the function of many other viral IRESs depends on specific sequences in apical stem-loops that in some cases make direct contact to the 40S ribosomal subunit (33–36). Although the apical loops of the HIV-1 gag IRES have functions during infection that are unrelated to translation initiation (37), we hypothesized that they are also important for IRES activity. To test this, we individually mutated the apical loops of the PBS, DIS, SD and PSI domains to an ultra-stable UUCG tetraloop in the context of dual-luciferase reporter constructs containing 1-384 nt of the gag leader (Figure 4A). The 5′-CUUCGG-3′ sequence maintains the secondary structure but alters the sequence within the apical loop (38,39). These loops are predicted to form in both secondary structure models (Figure 2A). In Jurkat T-cells, three of the four mutants had little effect on IRES activity, and mutant SD-A1 reduced the activity to ~55% of WT (Figure 4B). This result contrasts to what is observed for some other viral IRESs (such as HCV), where activity can drop to <10% of WT when apical loops are mutated (40). We conclude that the apical loops within the gag IRES do not play the same functionally critical role in driving recruitment of the translation machinery as they do in some other viral IRESs.

Helical elements and internal loops in the IRES have opposite effects on activity

Continuing to explore the roles of secondary structural elements within the IRES, we next targeted two helices and two internal loops (Figure 4A). Mutant PBS-H1 (designed to disrupt a helix) has ~2-fold higher activity than WT (Figure 4C). The increase in activity of this mutant is similar to mutant 132–384, which also lacks this helix owing to truncation of the 5′ end (Figure 2B). However, mutant PBS-H2 (designed to restore the helix) does not restore activity to WT levels (Figure 4C), suggesting that sequences within the helix, and not base pairing, are inhibitory. However, one caveat to this interpretation is that the degree to which PBS-H2 reforms the authentic secondary structure was not assessed. In the case of mutants PSI-H1 and PSI-H2, disruption of the helix leads to a 17% decrease in IRES activity (PSI-H2), whereas restoration of the helix (PSI-H1) restores the activity to above WT levels (Figure 4C). These data suggest that formation of the PSI helix is not critical for IRES function, and some sequence within this helix is inhibitory to IRES function. Again, this contrasts with other viral IRESs in which the active secondary and tertiary structure depends on formation of specific helices that organize the native fold.

To explore the role of two conserved internal loops found in the DIS stem-loop element, we mutated these loops in the context of 1–384 nt and tested the activity in the dual-luciferase reporter (Figure 4C). Mutation of the 'upper' loop to convert it to a helix (DIS-L1) decreased IRES activity by 28%, whereas mutations of bases within the loop to their Watson–Crick complements (DIS-L2) had little effect on activity. In contrast, similar mutations made to the 'lower' internal loop (DIS-L3 and DIS-L4) resulted in ~50% decrease in IRES activity. In particular, mutant DIS-L4, designed to maintain the presence of the internal loop but alter the sequence within it, showed the largest decrease in IRES activity of all the mutants we tested. Other mutations to this loop designed to favor alternate secondary structures show a similar loss of function (18), indicating that the sequence and perhaps the structural integrity of this internal loop is important for IRES function.

Taken together, our mutation data are consistent with the idea that the HIV-1 IRES is not as sensitive to mutations in individual secondary structure elements as are many other viral IRESs (15), although certain elements are more important than others. The mutations inducing the greatest negative effect on IRES activity are close to each other in sequence and secondary structure, that being the SD apical hairpin and the nearby 'lower' internal loop of the DIS stem-loop (Figure 4A; mutants SD-A1, DIS-L3 and DIS-L4). Likewise, a mutation made to the 5′-AAAA A-3′ sequence just downstream of the SD hairpin also decreases activity of the IRES to 60% of wild-type levels (18). These results are also in agreement with our truncation data, where deletion of nucleotides in this region decreases IRES activity (Figure 2C, compare 1–300 and 1–270 with 1–336). We conclude that this part of the gag leader, which surrounds a four-way junction in the 'U5:AUG' structural model but is more extended in the 'AUG hairpin' model (Figure 2A), may be among the most important for IRES activity.

Functionally important regions do not contain tightly packed RNA

Pre-folded four-way junctions are critical to organize the active 3D structure of the HCV IRES RNA (41), and thus the same may be true of the functionally important regions in the HIV-1 gag IRES. Although it has been proposed that HIV-1 gag IRES function is less dependent on RNA structure than are many other viral IRESs (15), this does not preclude that there are discrete regions of tightly packed RNA. Alternatively, the functionally important region might be conformationally dynamic, and this could be important for function. To directly discriminate between these two possibilities, we probed the gag IRES with hydroxyl radicals. These radicals cleave the RNA backbone in solvent-accessible regions, irrespective

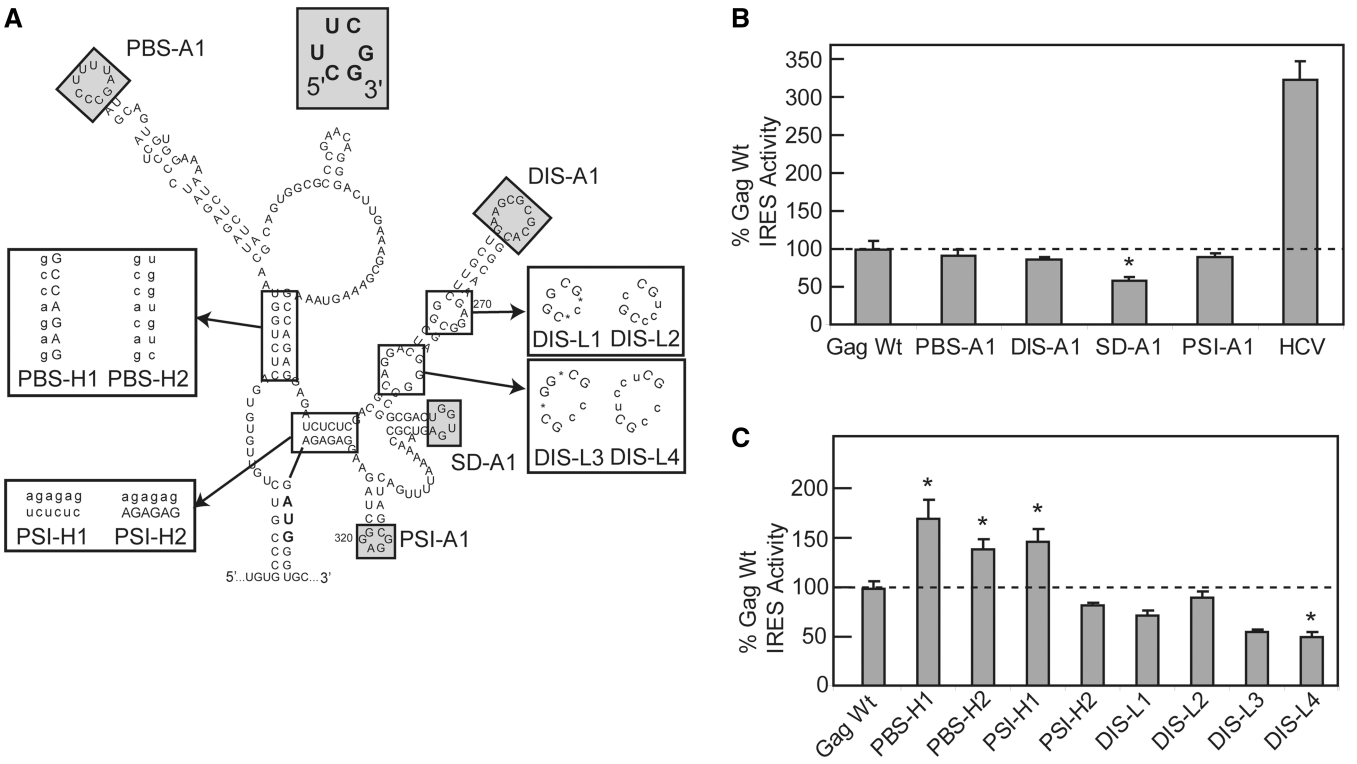

Figure 4. Role of secondary structures in IRES activity. (**A**) Secondary structure diagram (30) depicting the location and nature of mutations inserted into gag 1–384 of the dual luciferase vector (here, we are using the U5:AUG structure). Apical loops were mutated to a UUCG tetraloop (gray shading). Wild-type sequences are depicted by capital letters, mutations are lower case and asterisks denote deletions. The PBS, DIS, SD and PSI are labeled. (**B**) IRES activity was measured from Jurkat cells transfected with a dual-luciferase DNA construct containing HIV-1 gag 5′ leader (1–384 nts) apical loop mutants (depicted in A). Results are displayed as the averages of at least three independent transfections, plus SEM and are normalized to gag 1–384 (WT) levels. (**C**) Mutations in secondary structures were introduced into constructs containing the HIV-1 gag leader (1–384 nt), transfected into Jurkat cells and assayed for luciferase. Results are displayed as the averages of at least three independent transfections plus SEM and are normalized to gag 1–384 (WT). Significant changes in IRES activity in panels B and C are denoted with an asterisk ($P < 0.05$) based on a paired two-tailed student's *t*-test.

of secondary structure, but RNA involved in tight backbone packing is protected from cleavage. This method differs fundamentally from experiments designed to probe base pairing and secondary structure and has been used to query the ability of other IRES RNAs to fold into tight tertiary structures in the presence of Mg^{2+} (23,24). As a positive control, we subjected the HCV IRES to hydroxyl radical probing and observed specific backbone protections in the presence of Mg^{2+} (Figure 5A and B), indicative of tight backbone packing in discrete regions and matching previously reported protections (41). In contrast, hydroxyl radical probing on the HIV-1 IRES did not reveal any Mg^{2+}-induced changes in the cleavage pattern (Figure 5C and D), indicating that in the unbound form, the HIV-1 IRES does not adopt a magnesium-dependent tertiary fold even in the four-way junction. This result is consistent with the core IRES region being structurally plastic rather than tightly pre-folded.

In addition to gag, other HIV-1 transcripts can initiate translation internally

During infection, HIV-1 produces several alternatively spliced transcripts, each containing their own leader sequence, but common to all is a 289 nt non-coding exon at the 5′ end (hereafter referred to as the 'common exon'). In the case of the gag leader, we have shown that a construct (1–270) that is comprised only of RNA from the common exon retains robust IRES activity in Jurkat cells (Figure 2C). We therefore hypothesized that other common exon-containing HIV-1 transcripts could also initiate translation internally. To date, internal initiation from HIV-1 transcripts has only been reported for the 5′ leaders from the gag and tat mRNAs (20). Therefore, we inserted the entire 5′ leaders from the vpr (459 nts), vpu (374 nts), vif (418 nts) and nef (776 nts) transcripts into the dual-luciferase reporter vector and measured IRES activity in Jurkat T-cells. All leaders had IRES activity substantially greater (40–160-fold) than the negative control β-globin containing plasmid (Figure 6A). For reference, we included a gag truncation mutant (gag 1–270) to represent most of the common exon. Interestingly, despite containing the same first 270 nts, IRES activity varied from each leader. In one case (vpr), IRES activity was 20% lower than the levels we observed for the common exon, and in other cases (vif, vpu, nef), IRES activity was 22–175% greater. To ensure that apparent IRES activity was not a result of cryptic-processing events from the bicistronic plasmid, we again used

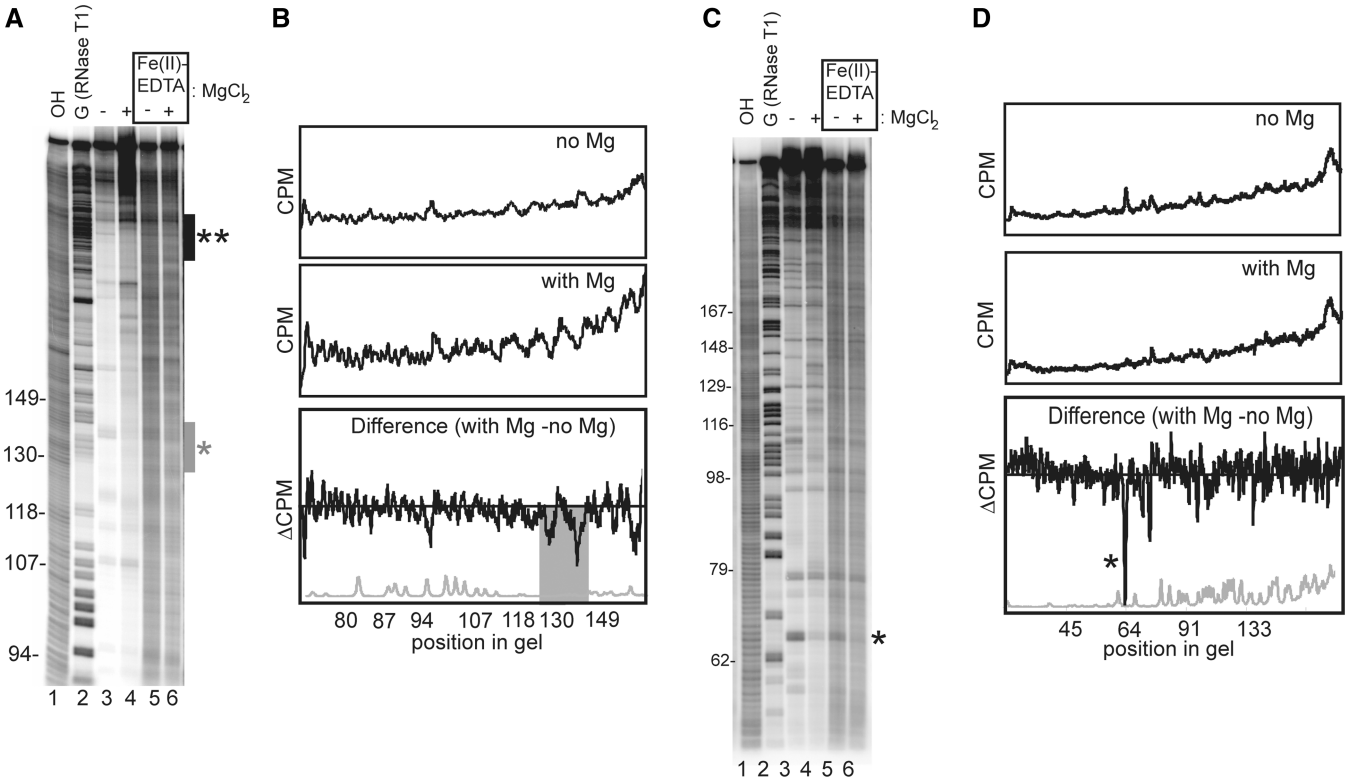

Figure 5. The HIV-1 gag IRES does not contain a Mg^{2+}-dependent tertiary fold. (**A**) Hydroxyl radical probing was performed on the HCV IRES, and cleavage products were run on a gel. Lane 1: OH ladder; cleaves at every nucleotide. Lane 2: RNase T1 ladder; cleaves at G nucleotides. Lanes 3 and 4: Cleavage products in the absence (lane 3) or presence (lane 4) of magnesium chloride, without the addition of radicals. Lanes 5 and 6: Cleavage products in the absence (lane 5) or presence (lane 6) of magnesium chloride, in the presence of radicals. Areas of significant protection from hydroxyl radical cleavage on the addition of magnesium are denoted by asterisks. A gray bar and single asterisk denote regions, which were quantified in (**B**). A black bar and double asterisk denotes a protected region, which was not quantified in this figure. (B) Quantified and normalized trace of the cleavage products in lanes 5 and 6 (top and middle panels) and the difference plots between the two (bottom panel). The trace from the T1 cleavages [lane 2 in (A)] is depicted on the bottom in gray, and nucleotide positions are also depicted. Areas shaded indicate regions of significant cleavage protection in the presence of magnesium and correspond with the single asterisk locations on the gel in (A). (**C**) Hydroxyl radical probing was performed on the HIV-1 gag IRES 1–384 nt, and cleavage products were run on a gel. The lane numbering and identification correlate with (A). Areas of a decreased non-radical induced cleavage on the addition of magnesium are denoted an asterisk. (**D**) Quantified and normalized trace of the cleavage products in lanes 5 and 6 (top and middle panels) of the HIV-1 probing and the difference plots between the two (bottom panel). The trace from the T1 cleavages [lane 2 (C)] is depicted on the bottom, and nucleotide positions are also depicted. Non-radical cleavage decreases in the presence of Mg^{2+} are depicted with an asterisk.

qPCR to measure the levels of FLUC and RLUC RNA (Figure 6B). FLUC and RLUC levels were equal for Nef, Vif, Vpr and Vpu constructs, as well as a negative control EMCV construct. In contrast, FLUC levels for Tau, an RNA leader known to contain a cryptic promoter and/or splice site was 2–3 times greater than RLUC. We also determined the sizes of LUC containing mRNAs produced after transfection using RT-PCR and observed single species of the expected size for dual-cistronic RNA, with no smaller products observed (Supplementary Figure S6). Together, these results suggest that apparent IRES activity for these leaders is not due to cryptic processing events and instead due to *bona fide* internal initiation. These results also suggest that although the common exon is used by all the leaders to drive internal translation initiation, the activity levels are modulated in the context of different leader sequences. The parts of the common exon that our mutational analysis showed to be important for gag IRES activity are just upstream of the location where the different transcripts are connected to the common exon. The mechanism by which these leaders initiate and regulate translation is under investigation.

DISCUSSION

HIV-1 RNAs are transcribed in the nucleus, processed and modified in a manner similar to cellular mRNAs. Despite being 5′ capped and 3′ polyadenylated, the HIV-1 gag leader has been reported to have IRES activity, including reports of changes in activity in response to the cell-cycle or stress (14,15,18). These features make the HIV-1 gag leader (and the HIV-1 family of transcripts in general) a useful model for understanding rules of IRES-driven translation initiation from diverse RNAs, including cellular. In general, IRES RNA function depends on multiple levels of RNA structure from primary sequence through higher-order three-dimensional structures, but our understanding is rudimentary regarding how different levels of IRES RNA structure and bound protein factors interplay to drive function and

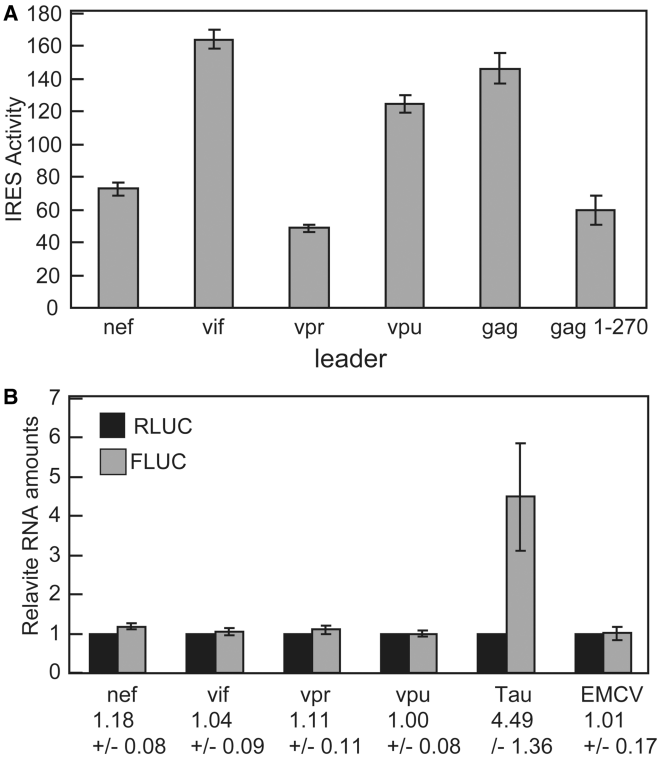

Figure 6. The activity of the HIV-1 IRES core is modulated by downstream sequences in other viral transcripts. (**A**). 5′ UTRs from the nef, vif, vpr and vpu transcripts were inserted in the dual-luciferase vector, and IRES activity was assayed in Jurkat cells. Results are displayed as the average of at least three independent experiments, plus the SEM and are normalized to β-globin, which was set at 1. The gag construct contains 1–336 nt (no ORF). A truncated leader (Gag 1–270) was included to represent IRES activity conferred by the common exon. (**B**) Results of quantitative PCR reactions. FLUC levels are displayed relative to RLUC and are averages of three independent experiments plus SEM. The average ratio RLUC:FLUC and SEM is included beneath each RNA species. FLUC and RLUC RNAs were not detected from cRNA reactions without RNA or reverse transcriptase non-transcribed regions of the plasmid or GAPDH were not detected, whereas transcribed regions of GAPDH were (data not shown).

regulate activity in diverse IRESs (42,43). Although it has been proposed that RNA structure is less important to function in the gag IRES than in other viral IRESs (15), we sought to rigorously examine this structure–function relationship. Our goal was to explore the link between RNA structure and activity within the HIV-1 gag IRES RNA in pathologically relevant cells, and in so doing to directly compare the characteristics of this IRES RNA with other viral IRESs known to be driven by RNA structure.

We first tested several human cell lines to determine which would support the most robust IRES activity, finding that within the confines of our system, the gag IRES is most active in T-cell and monocyte cell lines, which are derived from the natural cellular targets of HIV-1. We observed that the gag IRES is functional in Jurkat cells and activity was ~4-fold higher in these cells than in HeLa cells. The different gag IRES activities observed in different cell types raises the question of whether fundamentally different mechanisms and perhaps different regions of the gag leader are used to drive initiation in these various cells. We found that the minimal RNA sequence supporting internal initiation in Jurkat T-cells correlates well with a similar analysis performed in HeLa cells (14). In conjunction with the cell type analysis, these findings indicate that the fundamental RNA-dependent mechanism-driving IRES function from the HIV-1 gag leader is similar between HeLa and Jurkat T-cells, albeit with different activities.

The fact that IRES activity in HeLa and Jurkat T-cells depends on similar parts of the gag leader indicates that the RNA contains important functional determinants. Overall, we observe that most mutations designed to disrupt or alter specific secondary structure elements have only subtle effects on the activity of the IRES. However, mutations to the region at the base of the DIS stem-loop and surrounding the adjacent four-way junction had the greatest negative effects, suggesting this area is central to IRES function. Other studies also observed that IRES function is sensitive to mutations in this region, and this region of RNA is highly conserved among HIV-1 isolates, indicating an importance to the viral infection process that may reflect a role in translation initiation (18). However, our chemical probing reveals that this 'functional core' is not a compactly folded 'structural core', and thus we propose that the HIV-1 gag leader does not adopt a stable pre-formed tertiary fold *in vitro*. This finding agrees with hypotheses that there is a great deal of structural plasticity built into the leader RNA, and that this may allow the leader to change its configuration to perform diverse roles during infection (37). These studies support that the gag leader adopts at least two secondary structures, but we note that several of the elements we have identified as important for full IRES activity are the same in each (Figure 2A). This structural characteristic has implications for the mechanism of HIV-1 gag IRES function; specifically, it suggests that rather than being a direct manipulator of the translation machinery, the gag IRES function depends on binding of specific proteins that stabilize an IRES-active RNA structure (44–46). Furthermore, an important region for binding of these putative proteins is likely at the base of the DIS stem-loop and surrounding the adjacent four-way junction region. Indeed, this hypothesis is supported by a study that identified changes in the chemical probing profile of the IRES in this region on the addition of cell extract (15).

The fact that the HIV-1 gag IRES RNA is probably a flexible scaffold for protein binding combined with our result that the IRES has variable activities in different cells types suggests that some of the proteins used by the IRES are in higher abundance (or only present) in HIV-1 target cells. Consistent with this idea, the requirement for T-cell specific factors for viral processes is evident in both genome-wide shRNA screens and proteomic screens identifying factors, which either contribute to HIV-1 replication (47–50) or interact with HIV-1 viral proteins (51). In both cases, different factors were found when Jurkat, HeLa or Hek293 cells were used, suggesting that there are T-cell-specific factors used by HIV-1; some could enhance gag IRES-driven translation initiation.

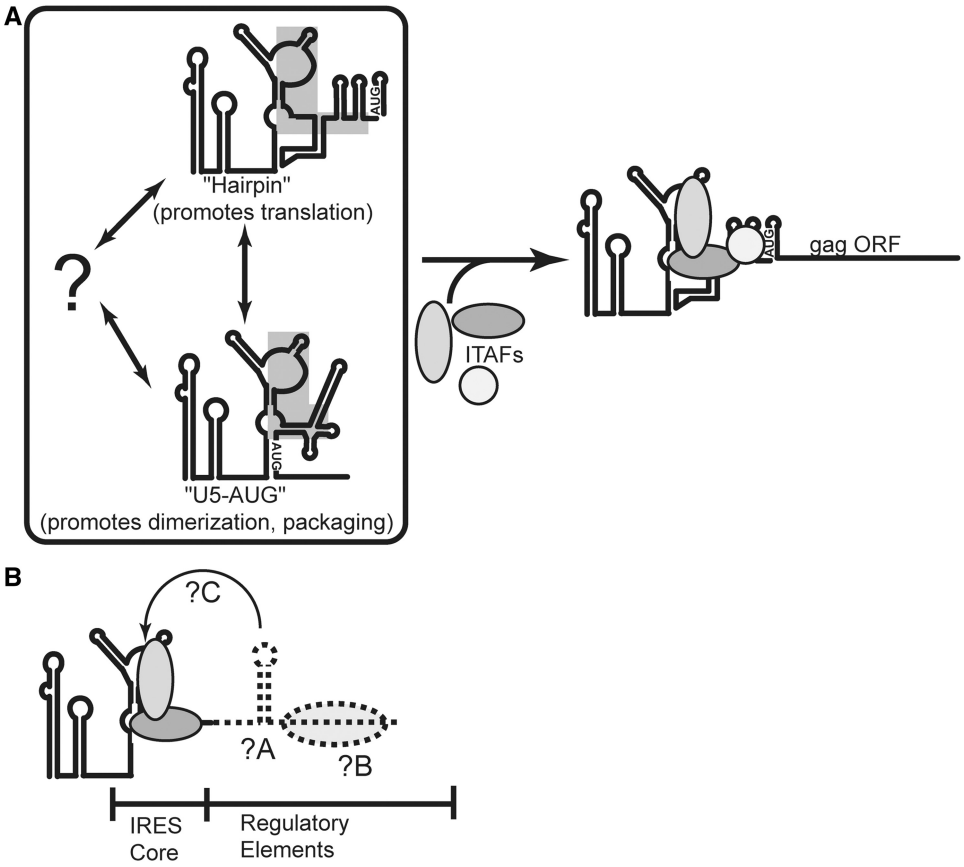

Figure 7. A model for IRES activity and modulation in HIV-1 transcripts. (**A**) We hypothesize that the HIV-1 gag leader can adopt several conformations and that different conformations promote different processes during infection. Here, we depict the U5-AUG and Hairpin conformations as cartoon diagrams (29) and depict with a question mark the possibility that additional conformations could exist. Of these possible structures, binding of cell type-specific ITAFs to the part of the leader that is most important for IRES activity (shaded boxes) stabilizes the conformation that drives IRES activity. (**B**) In transcripts other than gag, a similar mechanism is used in which ITAFs bind regions of the RNA common to all the transcripts, and the resultant structure is the Core IRES that drives activity in all the transcripts. The activity of translation initiation is then regulated by the different sequences added 3′ via alternative splicing (dashed lines, labeled as the regulatory element). Modulation by the regulatory element could occur through specific RNA structures formed in the regulatory element (A), through the binding of specific protein factors in this region (B), or through direct structural rearrangements of the core IRES by the regulatory element (**C**). It is also possible that a combination of these mechanisms leads to modulation of the core IRES element.

We identified cell-type specificity in the HIV-1 gag IRES in a context that differs from viral infection; whether cell type specificity of the IRES exists within the context of viral infection warrants further investigation. There is also clear precedent linking the cell type specificity of the HIV-1 gag IRES to cellular IRESs. In one example, the human c-myc IRES is not active in murine cells but is active in several human cell types, (52), and the neuron-specific family member (n-myc) has increased IRES activity in neuronal cell types compared with c-myc (53). In addition, our findings help explain why some other studies have not found evidence for an IRES in the gag leader (10,11). In one study, human cervical C33A cells were used to investigate the contribution of ribosomal scanning to the gag leader and concluded that the leader could not function as an IRES (10,11). Although we did not directly test these cells in our study, we would expect that like HeLa cells (which are also a cervical cell line) IRES activity from these cells would be less efficient than in the T-cell lines. Overall, these data reinforce the idea that IRESs have evolved to use the environment of certain cells, and care must be taken in drawing conclusions from experiments from a limited number of cell types. It also reinforces the fact that IRES RNAs could be used to regulate the expression of specific genes in specific cell types.

Based on the fact that all the HIV-1 viral transcripts contain a common exon that comprises the first 289 nts of each transcript, and the regions of RNA that drive internal initiation from the gag leader are largely found in this common exon, we predicted that other HIV-1 transcripts are capable of internal initiation. If true, this would provide an example of how alternatively spliced mRNAs arising from a single gene could use and regulate IRES function. Indeed, our data demonstrate that the 5′ leaders from vif, vpr, vpu and nef are functional IRESs, but that activity from each leader differs from the common exon alone. For vif, vpu and gag IRES activity is increased from what is observed from the common exon alone, whereas for vpr and nef, activity is similar to the common exon. Together, these results suggest that internal initiation from each leader is driven by the

common exon, and activity is modulated by nucleotides added onto the 3′ end. The finding of a common IRES element in multiple transcripts with differing activities has precedent. One example is the mouse trkB protein that can be expressed from a common IRES element found in two different 5′UTRs, L1 and L2 (54). Despite having a common element, each 5′UTR has a unique IRES activity that differs from the common element alone.

Our findings, combined with previously published results, lead to a speculative model for the role of RNA structure in the mechanism of internal initiation from the full-length gag transcript (Figure 7A). This model, although not fully tested, can form the basis for new hypotheses and further studies. In this model, the gag leader is a structurally plastic RNA capable of adopting several different conformations, consistent with the many tasks it must play during infection. As already noted, there is clear evidence that the gag leader can adopt at least two different conformations (29), and it seems possible that other uncharacterized structures could exist. Within the structurally dynamic leader are binding sites for proteins, including ITAFs that bind to the parts of the leader that we have mapped as important for IRES activity (Figure 7A; gray shaded boxes). These ITAFs select and stabilize the structure necessary for IRES activity. Precedent for ITAFs stabilizing tertiary structure is observed with two picornavirus IRESs (46,55), whereas evidence for ITAFs destabilizing structure is found in the Apaf-1 mRNA IRES (45). This model is consistent with studies in which addition of lysate altered the chemical probing pattern of regions in the leader that we find to be important for function, implying proteins have bound and altered the RNA structure (15). In addition, this model provides a hypothesis for the cell type dependence of gag IRES activity in that HIV-1 target cells may have a higher abundance of the required ITAFs than do non-target cells.

The speculative model for gag leader IRES activity can also be adapted and applied to the other HIV-1 transcripts (Figure 7B). Because all of these transcripts contain the common exon, they all contain RNA sequences that are primary drivers of IRES function (PBS, DIS regions). In our model, this common element is the 'IRES Core' that drives IRES activity in each leader, and this activity is then modulated in each leader by the unique nucleotides spliced to the 3′ end that act as regulatory elements. These regulatory elements could function by providing binding sites for trans-acting factors, causing a structural rearrangement of the IRES Core, by introducing new secondary structures, or they could use a combination of these mechanisms. Given that viral infection poses many stresses on the cell, which result in global inhibition of cap-dependent translation initiation (4–6), the ability to initiate both cap-dependently and internally, and to do so in a regulated manner, in multiple HIV-1 transcripts, may be a central, albeit unproven, component to the viral life cycle. By extension, this strategy could also be used by cellular mRNAs as a means to regulate translation of families of mRNAs generated by alternative splicing or with related, but not identical, leaders.

SUPPLEMENTARY DATA

Supplementary Data are available at NAR Online: Supplementary Table 1, Supplementary Figures 1–6 and Supplementary Methods.

ACKNOWLEDGEMENTS

The authors thank Mario Santiago, Marcelo Lopez-Lastra and Robert Batey for critical reading of this manuscript, Nahum Sonenberg for the HIV-1 gag IRES containing plasmid, the Krushel laboratory for additional plasmids and members of the Kieft Laboratory for useful discussions.

FUNDING

National Institutes of Health (NIH) [GM081346 to J.S.K., T32 AI052066 to T.D.M.P.]; American Heart Association [10PRE260143 to T.D.M.P.]. J.S.K. is an Early Career Scientist of the Howard Hughes Medical Institute. Funding for open access charge: NIH.

Conflict of interest statement. None declared.

REFERENCES

1. Balvay,L., Lopez Lastra,M., Sargueil,B., Darlix,J.L. and Ohlmann,T. (2007) Translational control of retroviruses. *Nat. Rev. Microbiol.*, **5**, 128–140.
2. Berkhout,B. (1996) Structure and function of the human immunodeficiency virus leader RNA. *Prog. Nucleic Acid. Res. Mol. Biol.*, **54**, 1–34.
3. Parkin,N.T., Cohen,E.A., Darveau,A., Rosen,C., Haseltine,W. and Sonenberg,N. (1988) Mutational analysis of the 5' non-coding region of human immunodeficiency virus type 1: effects of secondary structure on translation. *EMBO J.*, **7**, 2831–2837.
4. Jowett,J.B., Planelles,V., Poon,B., Shah,N.P., Chen,M.L. and Chen,I.S. (1995) The human immunodeficiency virus type 1 vpr gene arrests infected T cells in the G2 + M phase of the cell cycle. *J. Virol.*, **69**, 6304–6313.
5. Castello,A., Franco,D., Moral-Lopez,P., Berlanga,J.J., Alvarez,E., Wimmer,E. and Carrasco,L. (2009) HIV-1 protease inhibits Cap- and poly(A)-dependent translation upon eIF4GI and PABP cleavage. *PLoS One*, **4**, e7997.
6. Deshmane,S.L., Mukerjee,R., Fan,S., Del Valle,L., Michiels,C., Sweet,T., Rom,I., Khalili,K., Rappaport,J., Amini,S. *et al.* (2009) Activation of the oxidative stress pathway by HIV-1 Vpr leads to induction of hypoxia-inducible factor 1alpha expression. *J. Biol. Chem.*, **284**, 11364–11373.
7. Jackson,R.J. (2005) Alternative mechanisms of initiating translation of mammalian mRNAs. *Biochem. Soc. Trans.*, **33**, 1231–1241.
8. Komar,A.A. and Hatzoglou,M. (2011) Cellular IRES-mediated translation: the war of ITAFs in pathophysiological states. *Cell Cycle*, **10**, 229–240.
9. de Breyne,S., Soto-Rifo,R., Lopez-Lastra,M. and Ohlmann,T. (2013) Translation initiation is driven by different mechanisms on the HIV-1 and HIV-2 genomic RNAs. *Virus Res.*, **171**, 366–381.
10. Miele,G., Mouland,A., Harrison,G.P., Cohen,E. and Lever,A.M. (1996) The human immunodeficiency virus type 1 5′ packaging signal structure affects translation but does not function as an internal ribosome entry site structure. *J. Virol.*, **70**, 944–951.
11. Berkhout,B., Arts,K. and Abbink,T.E. (2011) Ribosomal scanning on the 5′-untranslated region of the human immunodeficiency virus RNA genome. *Nucleic Acids Res.*, **39**, 5232–5244.
12. Soto-Rifo,R., Rubilar,P.S., Limousin,T., de Breyne,S., Decimo,D. and Ohlmann,T. (2012) DEAD-box protein DDX3 associates

with eIF4F to promote translation of selected mRNAs. *EMBO J.*, **31**, 3745–3756.
13. Soto-Rifo,R., Limousin,T., Rubilar,P.S., Ricci,E.P., Decimo,D., Moncorge,O., Trabaud,M.A., Andre,P., Cimarelli,A. and Ohlmann,T. (2012) Different effects of the TAR structure on HIV-1 and HIV-2 genomic RNA translation. *Nucleic Acids Res.*, **40**, 2653–2667.
14. Brasey,A., Lopez-Lastra,M., Ohlmann,T., Beerens,N., Berkhout,B., Darlix,J.L. and Sonenberg,N. (2003) The leader of human immunodeficiency virus type 1 genomic RNA harbors an internal ribosome entry segment that is active during the G2/M phase of the cell cycle. *J. Virol.*, **77**, 3939–3949.
15. Vallejos,M., Deforges,J., Plank,T.D., Letelier,A., Ramdohr,P., Abraham,C.G., Valiente-Echeverria,F., Kieft,J.S., Sargueil,B. and Lopez-Lastra,M. (2011) Activity of the human immunodeficiency virus type 1 cell cycle-dependent internal ribosomal entry site is modulated by IRES trans-acting factors. *Nucleic Acids Res.*, **39**, 6186–6200.
16. Buck,C.B., Shen,X., Egan,M.A., Pierson,T.C., Walker,C.M. and Siliciano,R.F. (2001) The human immunodeficiency virus type 1 gag gene encodes an internal ribosome entry site. *J. Virol.*, **75**, 181–191.
17. Ricci,E.P., Soto Rifo,R., Herbreteau,C.H., Decimo,D. and Ohlmann,T. (2008) Lentiviral RNAs can use different mechanisms for translation initiation. *Biochem. Soc. Trans.*, **36**, 690–693.
18. Gendron,K., Ferbeyre,G., Heveker,N. and Brakier-Gingras,L. (2011) The activity of the HIV-1 IRES is stimulated by oxidative stress and controlled by a negative regulatory element. *Nucleic Acids Res.*, **39**, 902–912.
19. Purcell,D.F. and Martin,M.A. (1993) Alternative splicing of human immunodeficiency virus type 1 mRNA modulates viral protein expression, replication, and infectivity. *J. Virol.*, **67**, 6365–6378.
20. Charnay,N., Ivanyi-Nagy,R., Soto-Rifo,R., Ohlmann,T., Lopez-Lastra,M. and Darlix,J.L. (2009) Mechanism of HIV-1 Tat RNA translation and its activation by the Tat protein. *Retrovirology*, **6**, 74.
21. Stoneley,M., Paulin,F.E., Le Quesne,J.P., Chappell,S.A. and Willis,A.E. (1998) C-Myc 5′ untranslated region contains an internal ribosome entry segment. *Oncogene*, **16**, 423–428.
22. Filbin,M.E. and Kieft,J.S. (2011) HCV IRES domain IIb affects the configuration of coding RNA in the 40S subunit's decoding groove. *RNA*, **17**, 1258–1273.
23. Kieft,J.S., Zhou,K., Jubin,R., Murray,M.G., Lau,J.Y. and Doudna,J.A. (1999) The hepatitis C virus internal ribosome entry site adopts an ion-dependent tertiary fold. *J. Mol. Biol.*, **292**, 513–529.
24. Kieft,J.S., Costantino,D.A., Filbin,M.E., Hammond,J. and Pfingsten,J.S. (2007) Structural methods for studying IRES function. *Methods Enzymol.*, **430**, 333–371.
25. Locker,N., Chamond,N. and Sargueil,B. (2011) A conserved structure within the HIV gag open reading frame that controls translation initiation directly recruits the 40S subunit and eIF3. *Nucleic Acids Res.*, **39**, 2367–2377.
26. Veo,B.L. and Krushel,L.A. (2009) Translation initiation of the human tau mRNA through an internal ribosomal entry site. *J. Alzheimers Dis.*, **16**, 271–275.
27. Johannes,G., Carter,M.S., Eisen,M.B., Brown,P.O. and Sarnow,P. (1999) Identification of eukaryotic mRNAs that are translated at reduced cap binding complex eIF4F concentrations using a cDNA microarray. *Proc. Natl Acad. Sci. USA*, **96**, 13118–13123.
28. Chen,C.Y. and Sarnow,P. (1995) Initiation of protein synthesis by the eukaryotic translational apparatus on circular RNAs. *Science*, **268**, 415–417.
29. Lu,K., Heng,X., Garyu,L., Monti,S., Garcia,E.L., Kharytonchyk,S., Dorjsuren,B., Kulandaivel,G., Jones,S., Hiremath,A. *et al.* (2011) NMR detection of structures in the HIV-1 5′-leader RNA that regulate genome packaging. *Science*, **334**, 242–245.
30. Wilkinson,K.A., Gorelick,R.J., Vasa,S.M., Guex,N., Rein,A., Mathews,D.H., Giddings,M.C. and Weeks,K.M. (2008) High-throughput SHAPE analysis reveals structures in HIV-1 genomic RNA strongly conserved across distinct biological states. *PLoS Biol.*, **6**, e96.
31. de Breyne,S., Chamond,N., Decimo,D., Trabaud,M.A., Andre,P., Sargueil,B. and Ohlmann,T. (2012) *In vitro* studies reveal that different modes of initiation on HIV-1 mRNA have different levels of requirement for eukaryotic initiation factor 4F. *FEBS J.*, **279**, 3098–3111.
32. Valiente-Echeverria,F., Vallejos,M., Monette,A., Pino,K., Letelier,A., Huidobro-Toro,J.P., Mouland,A.J. and Lopez-Lastra,M. (2013) A cis-acting element present within the Gag open reading frame negatively impacts on the activity of the HIV-1 IRES. *PLoS One*, **8**, e56962.
33. Kieft,J.S., Zhou,K., Jubin,R. and Doudna,J.A. (2001) Mechanism of ribosome recruitment by hepatitis C IRES RNA. *RNA*, **7**, 194–206.
34. Kolupaeva,V.G., Pestova,T.V. and Hellen,C.U. (2000) An enzymatic footprinting analysis of the interaction of 40S ribosomal subunits with the internal ribosomal entry site of hepatitis C virus. *J. Virol.*, **74**, 6242–6250.
35. Jan,E. and Sarnow,P. (2002) Factorless ribosome assembly on the internal ribosome entry site of cricket paralysis virus. *J. Mol. Biol.*, **324**, 889–902.
36. Nishiyama,T., Yamamoto,H., Shibuya,N., Hatakeyama,Y., Hachimori,A., Uchiumi,T. and Nakashima,N. (2003) Structural elements in the internal ribosome entry site of Plautia stali intestine virus responsible for binding with ribosomes. *Nucleic Acids Res.*, **31**, 2434–2442.
37. Lu,K., Heng,X. and Summers,M.F. (2011) Structural determinants and mechanism of HIV-1 genome packaging. *J. Mol. Biol.*, **410**, 609–633.
38. Cheong,C., Varani,G. and Tinoco,I. Jr (1990) Solution structure of an unusually stable RNA hairpin, 5'GGAC(UUCG)GUCC. *Nature*, **346**, 680–682.
39. Tuerk,C., Gauss,P., Thermes,C., Groebe,D.R., Gayle,M., Guild,N., Stormo,G., d'Aubenton-Carafa,Y., Uhlenbeck,O.C., Tinoco,I. Jr *et al.* (1988) CUUCGG hairpins: extraordinarily stable RNA secondary structures associated with various biochemical processes. *Proc. Natl Acad. Sci. USA*, **85**, 1364–1368.
40. Jubin,R., Vantuno,N.E., Kieft,J.S., Murray,M.G., Doudna,J.A., Lau,J.Y. and Baroudy,B.M. (2000) Hepatitis C virus internal ribosome entry site (IRES) stem loop IIId contains a phylogenetically conserved GGG triplet essential for translation and IRES folding. *J. Virol.*, **74**, 10430–10437.
41. Kieft,J.S., Zhou,K., Jubin,R., Murray,M.G., Lau,J.Y. and Doudna,J.A. (1999) The hepatitis C virus internal ribosome entry site adopts an ion-dependent tertiary fold. *J. Mol. Biol.*, **292**, 513–529.
42. Filbin,M.E. and Kieft,J.S. (2009) Toward a structural understanding of IRES RNA function. *Curr. Opin. Struct. Biol.*, **19**, 267–276.
43. Plank,T.D. and Kieft,J.S. (2012) The structures of nonprotein-coding RNAs that drive internal ribosome entry site function. *Wiley Interdiscip. Rev. RNA*, **3**, 195–212.
44. Pickering,B.M., Mitchell,S.A., Spriggs,K.A., Stoneley,M. and Willis,A.E. (2004) Bag-1 internal ribosome entry segment activity is promoted by structural changes mediated by poly(rC) binding protein 1 and recruitment of polypyrimidine tract binding protein 1. *Mol. Cell Biol.*, **24**, 5595–5605.
45. Mitchell,S.A., Spriggs,K.A., Coldwell,M.J., Jackson,R.J. and Willis,A.E. (2003) The Apaf-1 internal ribosome entry segment attains the correct structural conformation for function via interactions with PTB and unr. *Mol. Cell*, **11**, 757–771.
46. Kafasla,P., Morgner,N., Poyry,T.A., Curry,S., Robinson,C.V. and Jackson,R.J. (2009) Polypyrimidine tract binding protein stabilizes the encephalomyocarditis virus IRES structure via binding multiple sites in a unique orientation. *Mol. Cell*, **34**, 556–568.
47. Konig,R., Zhou,Y., Elleder,D., Diamond,T.L., Bonamy,G.M., Irelan,J.T., Chiang,C.Y., Tu,B.P., De Jesus,P.D., Lilley,C.E. *et al.* (2008) Global analysis of host-pathogen interactions that regulate early-stage HIV-1 replication. *Cell*, **135**, 49–60.
48. Yeung,M.L., Houzet,L., Yedavalli,V.S. and Jeang,K.T. (2009) A genome-wide short hairpin RNA screening of jurkat T-cells for human proteins contributing to productive HIV-1 replication. *J. Biol. Chem.*, **284**, 19463–19473.
49. Zhou,H., Xu,M., Huang,Q., Gates,A.T., Zhang,X.D., Castle,J.C., Stec,E., Ferrer,M., Strulovici,B., Hazuda,D.J. *et al.* (2008)

Genome-scale RNAi screen for host factors required for HIV replication. *Cell Host Microbe*., **4**, 495–504.
50. Brass,A.L., Dykxhoorn,D.M., Benita,Y., Yan,N., Engelman,A., Xavier,R.J., Lieberman,J. and Elledge,S.J. (2008) Identification of host proteins required for HIV infection through a functional genomic screen. *Science*, **319**, 921–926.
51. Jager,S., Cimermancic,P., Gulbahce,N., Johnson,J.R., McGovern,K.E., Clarke,S.C., Shales,M., Mercenne,G., Pache,L., Li,K. *et al*. (2012) Global landscape of HIV-human protein complexes. *Nature*, **481**, 365–370.
52. Stoneley,M., Subkhankulova,T., Le Quesne,J.P., Coldwell,M.J., Jopling,C.L., Belsham,G.J. and Willis,A.E. (2000) Analysis of the c-myc IRES; a potential role for cell-type specific trans-acting factors and the nuclear compartment. *Nucleic Acids Res*., **28**, 687–694.
53. Jopling,C.L. and Willis,A.E. (2001) N-myc translation is initiated via an internal ribosome entry segment that displays enhanced activity in neuronal cells. *Oncogene*, **20**, 2664–2670.
54. Timmerman,S.L., Pfingsten,J.S., Kieft,J.S. and Krushel,L.A. (2008) The 5' leader of the mRNA encoding the mouse neurotrophin receptor TrkB contains two internal ribosomal entry sites that are differentially regulated. *PLoS One*, **3**, e3242.
55. Yu,Y., Abaeva,I.S., Marintchev,A., Pestova,T.V. and Hellen,C.U. (2011) Common conformational changes induced in type 2 picornavirus IRESs by cognate trans-acting factors. *Nucleic Acids Res*., **39**, 4851–4865.